Electronic Supplementary Material (ESI) for Green Chemistry.

Table of contents

1. Experimental details

1.1. Material synthesis

To prepare CoPPc-CNT, 100 mg of CNTs were dispersed in 80 mL deionized water or ethanol with the assistance of >30 min sonication. 1,2,4,5-tetracyanobenzene (100 mg), anhydrous $CoCl_2$ (36 mg), and 1,8-diazabicyclo[5.4.0] undec-7-ene (86 mg) were then added and dispersed with additional 30 min sonication. The mixture was transferred to a Teflon lined autoclave for hydrothermal heating at 180°C for 8 hr. The final product was collected by centrifugation at 8,000 rpm, then washed with ethanol and water and finally freeze dried. Pure CoPPc was similarly prepared but excludes CNTs.

To prepare defective catalyst (D-CoPPc-CNT), 100 mg of CNTs were dispersed in 80 mL ethanol with the assistance of >30 min sonication. 1,2-dicyanobenzene/1,2,4,5-tetracyanobenzene (100 mg in total), anhydrous $CoCl_2$ (36 mg), and 1,8-diazabicyclo[5.4.0] undec-7-ene (86 mg) were then added and dispersed with additional 30 min sonication. The mixture was transferred to a Teflon lined autoclave for hydrothermal heating at 180°C for 8 hr. The final product was collected by centrifugation at 8,000 rpm, then washed with ethanol and water and finally freeze dried.

1.2. Material characterizations

TEM. The morphology and elemental distributions of CoPPc-CNT were characterized with a Transmission Electron Microscopy (JEM 2100f) equipped with an EDS detector and operated at an accelerating voltage of 200 kV. Samples were firstly suspended in ethanol with the assistance of 30 min sonication. Then 6-8 drops of the mixture were deposited on a copper microscope grid (Beijing Zhongjingkeyi Technology) and dried overnight.

Raman. Raman spectrum were collected using a confocal Raman spectroscopy (LabRAM HR, Horiba J.Y., France) equipped with a visible 514.5 nm Ar+ laser, a high-grade Leica microscope (long working distance objective 50×) and a deep-depleted thermoelectrically cooled CCD array detector (1024×256 pixels, 26 mm in size).

FT-IR. Fourier transform infrared (FT-IR) spectra were measured with an FT-IR spectrometer (Perkin-Elmer, Model Spectrum 100). Samples were mixed with KBr powder (Spectral purity) at a sample/KBr weight ratio of 1/2000. The mixture was then ground to 100 mesh size and pressed into a lucency disk, which was then directly placed into the IR spectrometer for measurement within the frequency range of 4000–450 cm^{-1}.

XRD. The X-ray powder diffraction (XRD) pattern of CoPPc-CNT was measured with a Bruker D8 Advance diffractometer using a CuKa ray source (λ=0.154 nm) for continuous scanning with accelerated voltage 40 kV and 40 mA detector current in an angular range of 10°–80°.

ICP. ICP-atomic emission spectroscopy measurements were conducted with an Agilent 725 ICP-OES. Samples were first digested in concentrated HNO_3 and then decomposed with digestion instrument at 120°C. The suspension was filtered, and the supernatant was diluted to desired concentrations for analysis.

XPS. X-ray photoelectron spectroscopy (XPS) analysis was performed on a Thermo ESCALAB 250Xi spectrometer using a monochromatic AlK radiation source (1486.6 eV, pass energy 20.0 eV). The binding energies (BEs) were calibrated using the C1s peak at 284.8 eV as a reference.

Conductivity measurement. The electronic conductivity of the catalysts was measured with a four-probe resistance square resistance tester (Helpass HPS2523) at room temperature.

Contact angle measurement. The hydrophilicity was evaluated with a contact angle measuring instrument (JC2000D). A drop of deionized water drip on a pressed catalyst wafer and the images were recorded once per second with a high-speed camera.

1.3. Working electrode preparation

To prepare the working electrode, 4 mg of CoPPc-CNT, 10 uL of 5 wt.% Nafion solution were dispersed in 2 mL of ethanol and sonicated for 30 min to form a uniform catalyst ink. The suspension was then drop cast onto carbon paper disk (Toray, TGP-H-060) to achieve a CoPPc-CNT loading of 45 ug/cm^2.

1.4. Electrochemical measurements

The electrochemical performance for CO_2 reduction was tested in a customized H-type cell separated by a Nafion-117 membrane. A platinum foil was used as a counter electrode and a leak-free Ag/AgCl electrode (LF-2, Innovative Instrument Inc) was used as reference electrode. Prior to experiments, 1.75 mL of electrolyte was added into the working and counter compartment, respectively. Cells were purged with CO_2 for 10 min prior to electrochemical tests. A CHI650E potentiostat was employed to record the electrochemical response. Resistance of electrolyte between reference electrode and working electrode was measured with Potential Electrochemical Impedance Spectroscopy (PEIS) and manually compensated. During constant-potential electrolysis, gas products were analyzed by an on-line gas chromatograph (Ruimin GC 2060, Shanghai) equipped with TCD and FID detectors, a methanizer, and a Hayesep-D column.

2. Supplementary figures

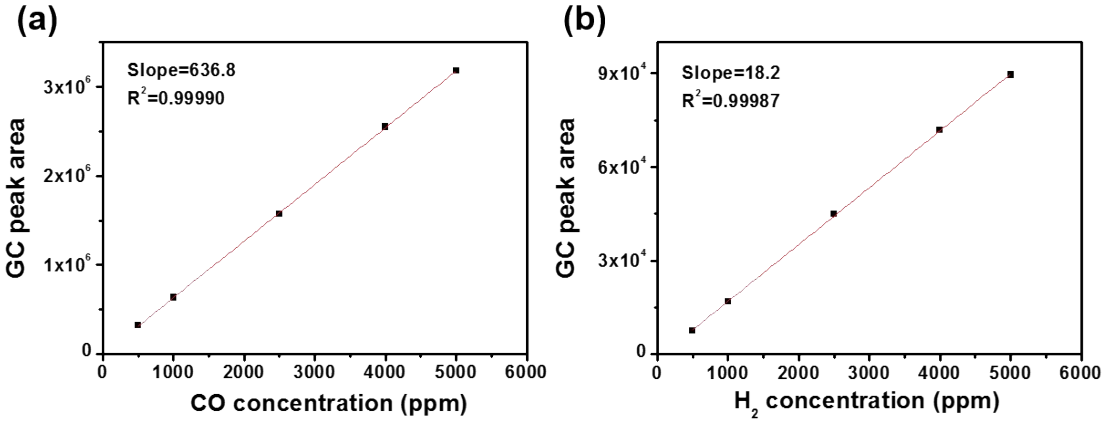

Figure S1. Calibration curve for (a) CO and (b) H_2.

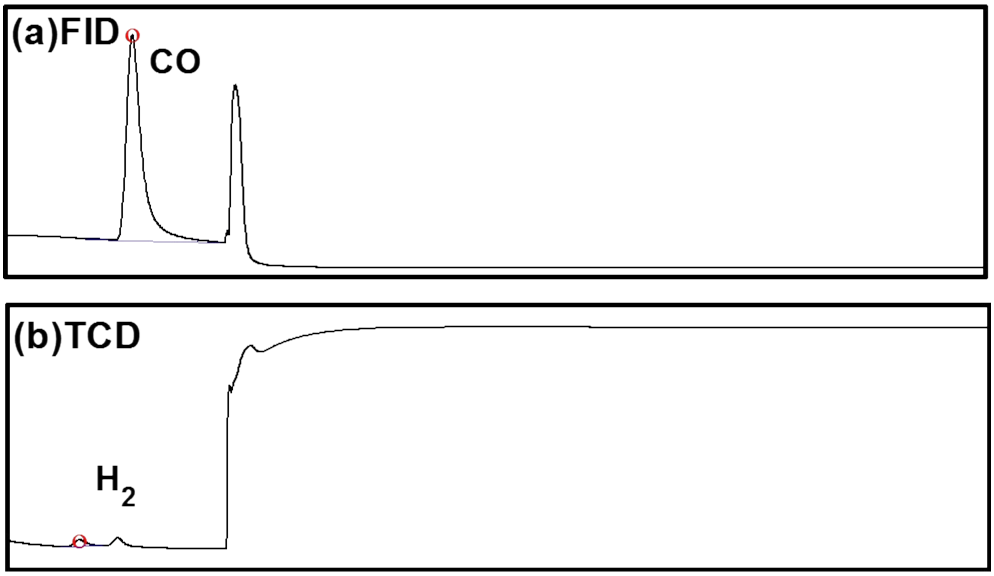

Figure S2. Sample GC signal showing (a) CO from FID detector and (b) H_2 from TCD detector during a common steady-state electrolysis measurement.

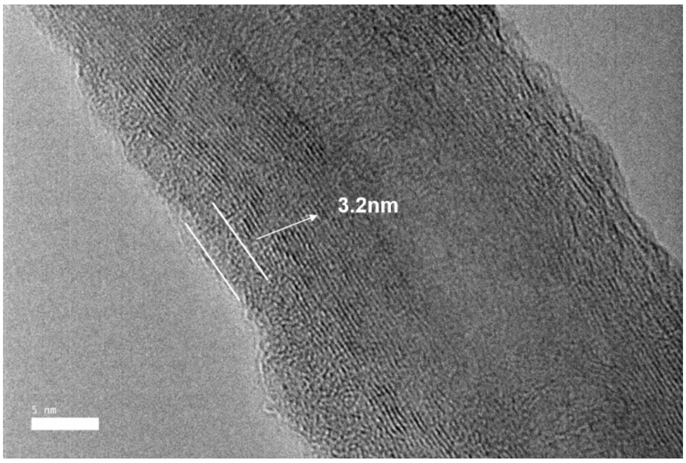

Figure S3. TEM image of CoPPc-CNT(20-30) that is dried in an ordinary oven.

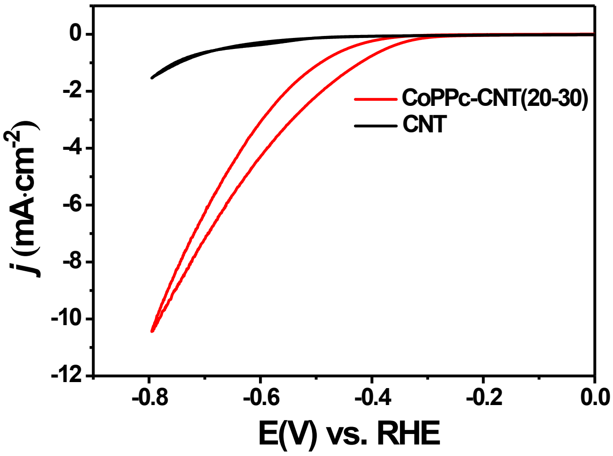

Figure S4. Cyclic voltammograms recorded at a sweep rate of 10 mV/s on CoPPc-CNT (20-30) and CNT.

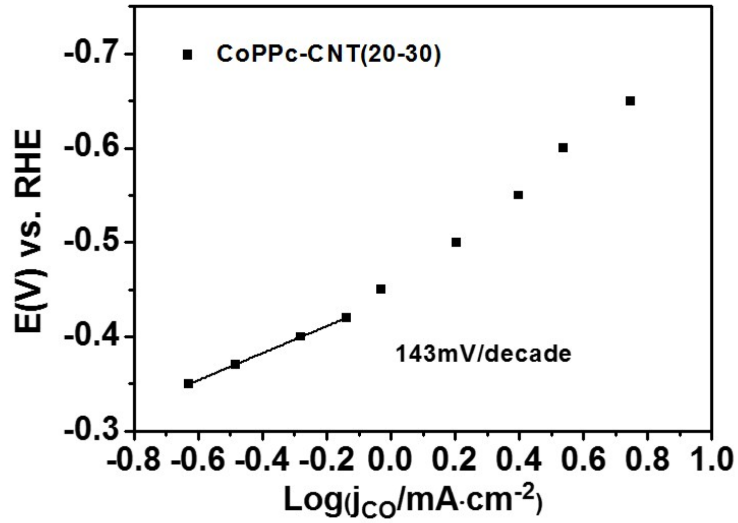

Figure S5. Tafel plots for CoPPc-CNT(20-30) in 0.5 M $NaHCO_3$ electrolyte.

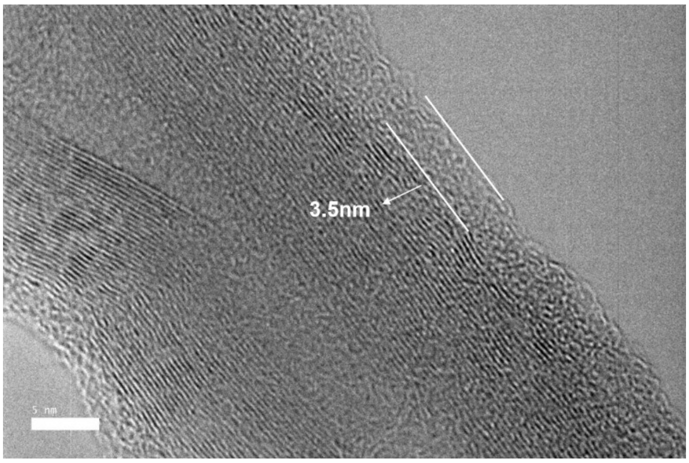

Figure S6. TEM image of CoPPc-CNT(20-30) after the long-term stability test.

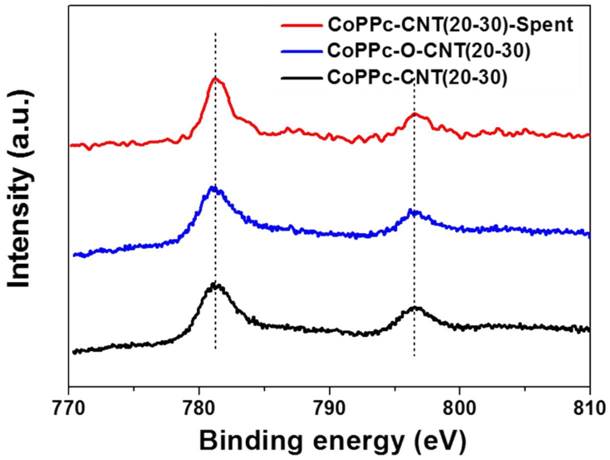

Figure S7. Co 2p spectra of CoPPc-CNT(20-30), CoPPc-O-CNT(20-30) and CoPPc-CNT(20-30) after the long-term stability test.

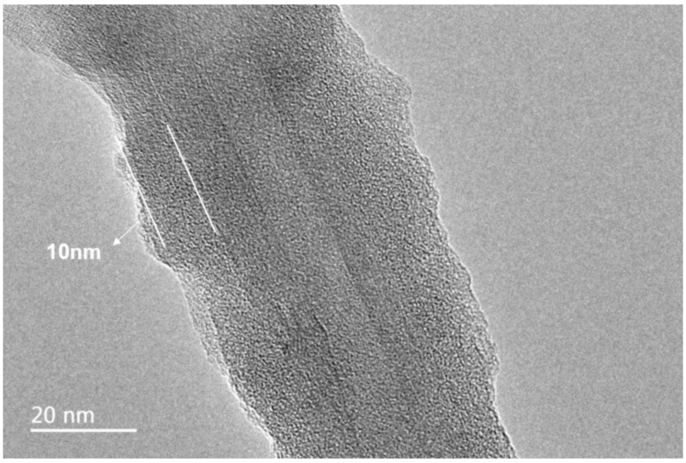

Figure S8. TEM image of CoPPc-CNT(30-50) .

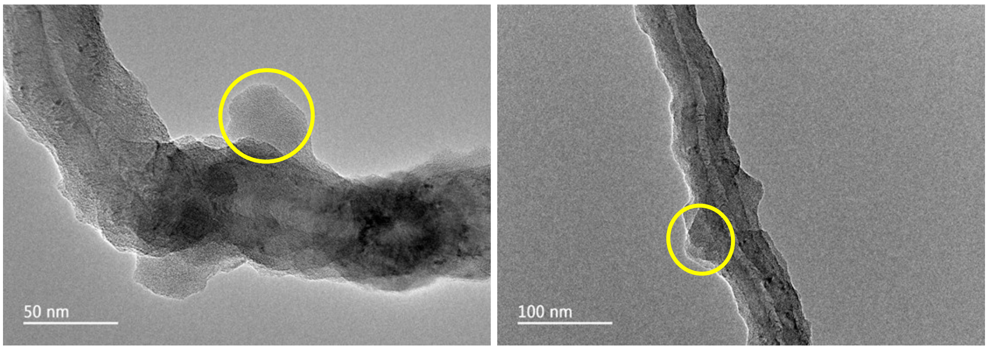

Figure S9. TEM image of CoPPc-CNT(10-20) showing the existence of aggregations.

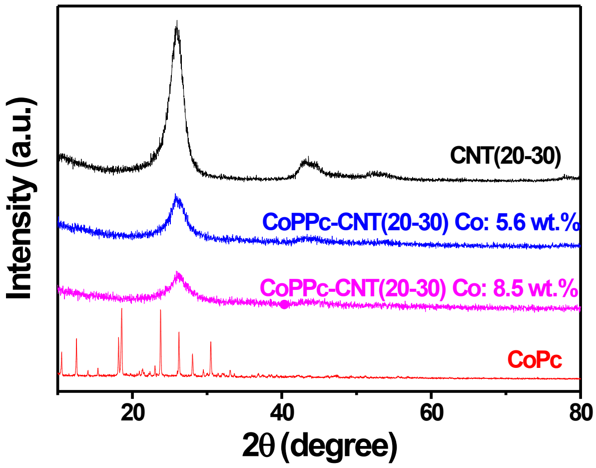

Figure S10. XRD pattern of CoPPc-CNT (20-30), commercial CoPc, and pure CNT(20-30)

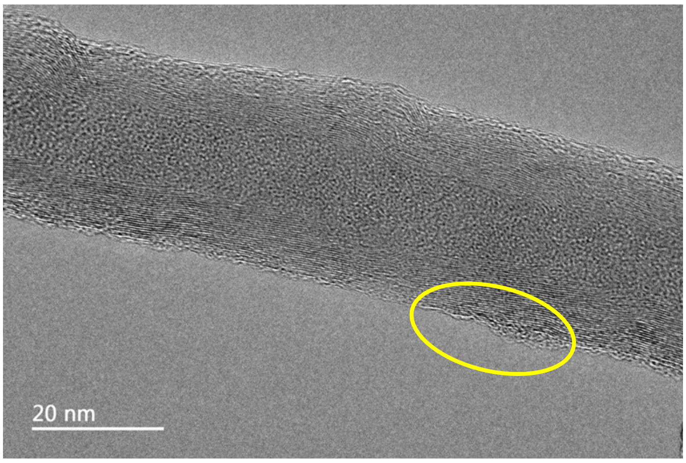

Figure S11. TEM image of CoPPc-CNT(20-30) showing the partial exposure of CNTs.

(Co loading: 4.1 wt.%)

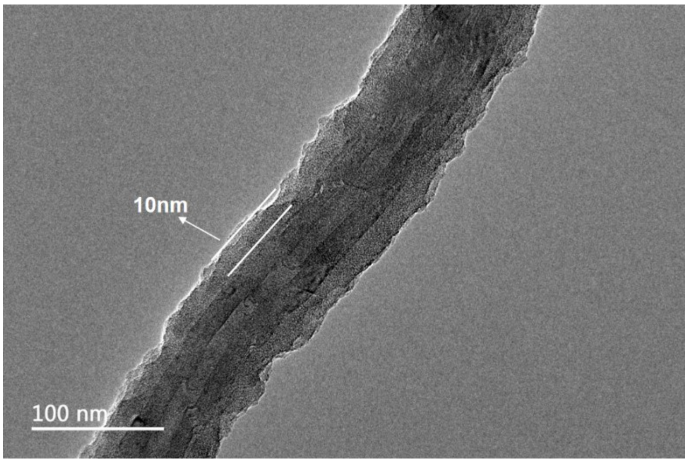

Figure S12. TEM image of CoPPc-CNT(20-30) showing thick polymer layer.

(Co loading: 8.5 wt.%)

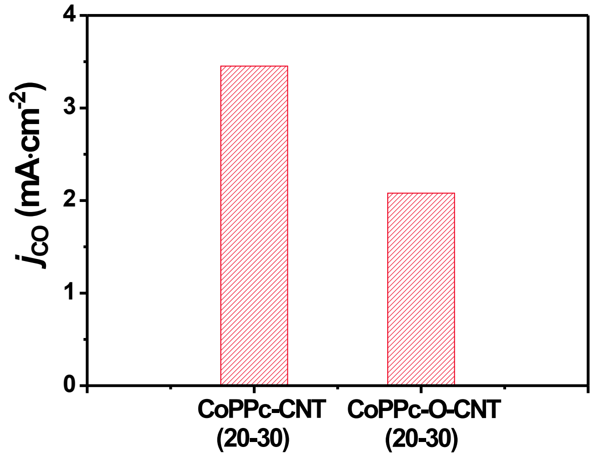

Figure S13. CO partial current densities of CoPPc-CNT(20-30) and CoPPc-O-CNT(20-30) at -0.6 V *vs.* RHE.

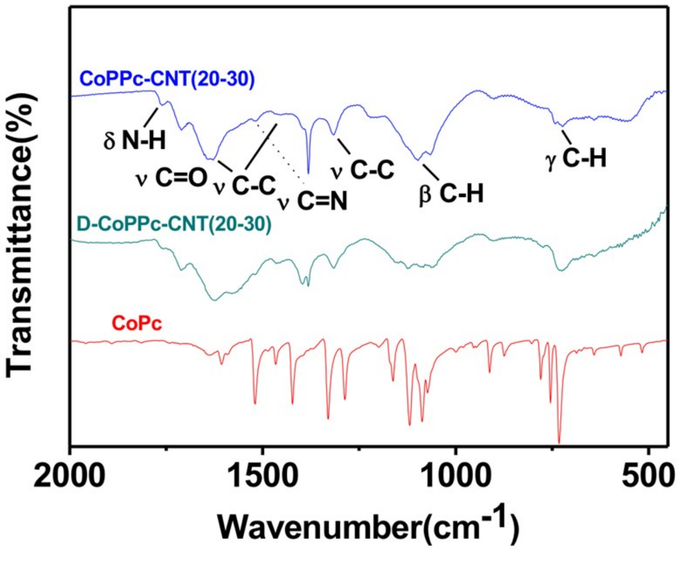

Figure S14. FT-IR spectra of CoPPc-CNT(20-30), D-CoPPc-CNT(20-30) and commercial CoPc.

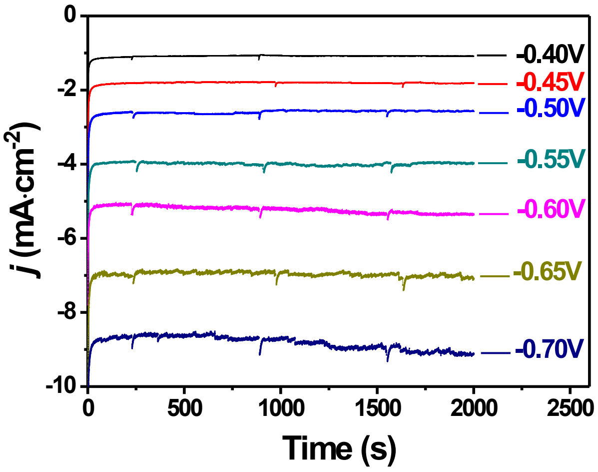

Figure S15. Overall current densities for electrochemical CO_2 reduction catalyzed by D-CoPPc-CNT(20-30) at various potentials.

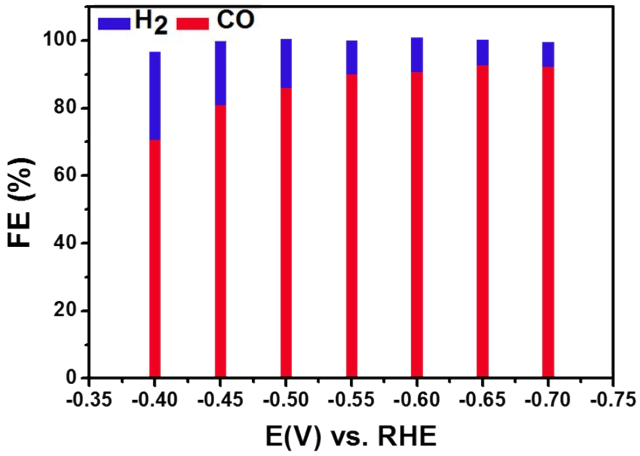

Figure S16. Faradaic efficiencies of electrochemical CO_2 reduction catalyzed by the D-CoPPc-CNT(20-30) at various potentials.

3. Supplementary tables

Table S1. Electrochemical performances of CoPPc-CNT(20-30) synthesized in ethanol and water.

Catalyst	**Potential (V vs. RHE)**	**Current density (mA/cm^2)**	**Faradaic efficiency(%)**		**Normalized loading (mA/mg_{cat})**
			CO	**H_2**	
CoPPc-CNT (20-30)-e	-0.60	-3.6	96.0	4.5	79.6
CoPPc-CNT (20-30)-w	-0.60	-3.5	94.4	5.8	77.4
CoPPc-CNT (20-30)-oven	-0.60	-3.7	96.2	3.9	81.8
Unsupported CoPPc	-0.60	-1.1	55.4	44.0	24.3

e:ethanol as the solvent; w: water as the solvent; oven: dried in an ordinary oven

Table S2. Reactants for CoPPc-CNT(20-30) with polymer loadings.

Catalyst	**Composition (mg)**			**Co (%)**	**Conductivity (S/cm)**
	CNT	**1,2,4,5-benzenetetracarbonitrile**	**$CoCl_2$**		
Cat-1	100	75	27	4.1	5
Cat-2	100	100	36	5.6	2.1
Cat-3	100	125	45	6.3	0.8
Cat-4	100	150	54	7.2	0.4
Cat-5	100	200	72	8.5	0.02
Cat-6	100	100	36	-	0.3

Cat-1, 2, 3, 4, 5: CoPPc-CNT (20-30) with different surface polymer and carbon support mass ratio: 0.75, 1, 1.25, 1.5, 2; Cat-6: CoPPc-O-CNT(20-30)

Table S3. Atomic content of heteroatom-doped CNT based on XPS survey characterization.

Element (%)	**C**	**N**	**O**
CNT	98.76	0	1.24
O-CNT	94.15	0.4	5.44

Table S4. Cobalt content of D-CoPPc-CNT with different M2/(M1+M2) ratio.

M2/(M1+M2)	0	0.25	0.5	0.75	1
Co (wt.%)	5.6	7.4	8.8	9.3	9.1

Table S5. A comparison of reported molecular catalysts for the electroreduction of CO_2 to CO in aqueous media to CoPPc-CNT(20-30).

Catalyst	*j* (mA/cm^2)	V vs. RHE	Electrolyte (pH)	FE$_{CO}$ (%)	TOF$_{CO}$ (s^{-1})	specific activity (mA/mg$_{cat}$)	Ref.
CoPPc-CNT(20-30)	3.6	-0.60	0.5M $NaHCO_3$ (7.3)	96	0.41	79.6	This work
D-CoPPc-CNT(20-30)	5.6	-0.60	0.5M $NaHCO_3$ (7.3)	91	0.39	123.8	This work
CoPPc/CNT	~18.0	-0.61	0.5M $NaHCO_3$ (7.3)	90	1.4	18	[1]
D-P-CoPc	2.5	-0.60	0.5M $KHCO_3$ (7.3)	97	0.11	2.5	[2]
CoPP@CNT	25.1	-0.60	0.5M $NaHCO_3$ (7.3)	98.3	1.9	50.2	[3]
CoPc-py-CNT	5.5	-0.63	0.2M $KHCO_3$ (7.0)	98.4	4.9	88.6	[4]
CoPc/CNT	10	-0.63	0.1M $KHCO_3$ (6.8)	92	2.7	24.7	[5]
CoPc-CN/CNT	15	-0.63	0.1M $KHCO_3$ (6.8)	98	4.1	37.5	[5]
CoPc-CN/CNT	5.6	-0.46	0.5M $KHCO_3$ (7.2)	88	1.4	12.8	[5]
CoPc-P4VP	2.0	-0.73	0.1 M NaH_2PO_4 (4.7)	89	4.8	NA	[6]
CoPc(py)-P2VP	1.9	-0.73	0.1 M NaH_2PO_4 (4.7)	83	4.2	NA	[6]
CATpyr/CNT	0.24	-0.59	0.5M $KHCO_3$ (7.3)	93	0.04	2.0	[7]
CoTPP–CNT	NR	-0.66	0.5M $KHCO_3$ (7.2)	70	2.75	NA	[8]
Coqpy	10	-0.48	0.5M $KHCO_3$ (7.3)	100	5.9	100	[9]
CoPc-F	6.0	-0.90	0.5M $KHCO_3$ (7.2)	88	2.05	NA	[10]
Al2(OH)$_2$TCPP-Co	1.0	-0.67	0.5M $KHCO_3$ (7.3)	76	0.06	NA	[11]
COF-367-Co	3.3	-0.67	0.5M $KHCO_3$ (7.3)	91	0.53	NA	[12]
COF-367-Co(1%)	0.45	-0.67	0.5M $KHCO_3$ (7.3)	53	2.6	NA	[12]

(N.A. is not available.)

4. Supplementary discussions

4.1. Derivation of theoretical monolayer coverage

The calculation is made based on (i) surface area of carbon nanotubes is measured by BET to be 230 m^2 /g; (ii) polymerized CoPc forms a two-dimensional network on the surface of CNT and (iii) dimension of an optimized lattice parameters for the CoPPc layer are a = b = 1.0 nm.[13]

Monolayer Co content (wt.%)

$$= \frac{Surface\ area\ of\ CNT}{Doninating\ area\ of\ CoPc\ molecule} \times \frac{molecular\ weight\ of\ Co\ at}{N_A}$$

$$\times \frac{58.933 g \cdot mol^{-1}}{6.02 \times 10^{23}}$$

$$= 2.25\ wt.\%$$

5. References

[1] N. Han, Y. Wang, L. Ma, J. Wen, J. Li, H. Zheng, K. Nie, X. Wang, F. Zhao, Y. Li, J. Fan, J. Zhong, T. Wu, D. J. Miller, J. Lu, S.-T. Lee, Y. Li, *Chem* **2017**, *3*, 652-664.

[2] H. Wu, M. Zeng, X. Zhu, C. Tian, B. Mei, Y. Song, X.-L. Du, Z. Jiang, L. He, C. Xia, S. Dai, *ChemElectroChem* **2018**, *5*, 2717-2721.

[3] M. Zhu, J. Chen, L. Huang, R. Ye, J. Xu, Y. F. Han, *Angew Chem Int Ed Engl* **2019**.

[4] M. Zhu, J. Chen, R. Guo, J. Xu, X. Fang, Y.-F. Han, *Applied Catalysis B: Environmental* **2019**, *251*, 112-118.

[5] X. Zhang, Z. Wu, X. Zhang, L. Li, Y. Li, H. Xu, X. Li, X. Yu, Z. Zhang, Y. Liang, H. Wang, *Nat Commun* **2017**, *8*, 14675.

[6] W. W. Kramer, C. C. L. McCrory, *Chem Sci* **2016**, *7*, 2506-2515.

[7] A. Maurin, M. Robert, *J Am Chem Soc* **2016**, *138*, 2492-2495.

[8] X. M. Hu, M. H. Ronne, S. U. Pedersen, T. Skrydstrup, K. Daasbjerg, *Angew Chem Int Ed Engl* **2017**, *56*, 6468-6472.

[9] M. Wang, L. Chen, T.-C. Lau, M. Robert, *Angewandte Chemie International Edition* **2018**, *57*, 7769-7773.

[10] N. Morlanés, K. Takanabe, V. Rodionov, *ACS Catalysis* **2016**, *6*, 3092-3095.

[11] N. Kornienko, Y. Zhao, C. S. Kley, C. Zhu, D. Kim, S. Lin, C. J. Chang, O. M. Yaghi, P. Yang, *J Am Chem Soc* **2015**, *137*, 14129-14135.

[12] S. Lin, C. S. Diercks, Y. B. Zhang, N. Kornienko, E. M. Nichols, Y. Zhao, A. R. Paris, D. Kim, P. Yang, O. M. Yaghi, C. J. Chang, *Science* **2015**, *349*, 1208-1213.

[13] Y. Wang, H. Yuan, Y. Li, Z. Chen, *Nanoscale* **2015**, *7*, 11633-11641.